Neutrosophic C-Means Clustering with Optimal Machine Learning Enabled Skin Lesion Segmentation and Classification

Fatma Taher [1,*], Ahmed Abdelaziz [2]

[1] College of Technological Innovation, Zayed University, Dubai, UAE
[2] Nova Information Management School, Universidade Nova de Lisboa, 1070-312, Lisboa, Portugal
[2] Information System Department, Higher Technological Institute, HTI, Cairo 44629, Egypt
Emails: Fatma.Taher@zu.ac.ae; D20190535@novaims.unl.pt

Abstract

Early detection and classification of skin lesions using dermoscopic images have attracted significant attention in the healthcare sector. Automated skin lesion segmentation becomes tedious owing to the presence of artifacts like hair, skin line, etc. Earlier works have developed skin lesion detection models using clustering approaches. The advances in neutrosophic set (NS) models can be applied to derive effective clustering models for skin lesion segmentation. At the same time, artificial intelligence (AI) tools can be developed for the identification and categorization of skin cancer using dermoscopic images. This article introduces a Neutrosophic C-Means Clustering with Optimal Machine Learning Enabled Skin Lesion Segmentation and Classification (NCCOML-SKSC) model. The proposed NCCOML-SKSC model derives a NCC-based segmentation approach to segment the dermoscopic images. Besides, the AlexNet model is exploited to generate a feature vector. In the final stage, the optimal multilayer perceptron (MLP) model is utilized for the classification process in which the MLP parameters are chosen by the use of a whale optimization algorithm (WOA). A detailed experimental analysis of the NCCOML-SKSC model using a benchmark dataset is performed and the results highlighted the supremacy of the NCCOML-SKSC model over the recent approaches.

Keywords: Image segmentation; Neutrosophic set; Feature Extraction; Machine learning; Whale optimization algorithm.

1. Introduction

Medical examination has shown that skin cancer is a significant general medical issue. It is assessed that one of every five Americans might be impacted by skin cancer [1]. Melanoma is one of the most well-known types and risky skin cancer. Early identification and precise finding of the skin lesion is pivotal, specifically for melanoma. Dermoscopic assessment of melanocytic lesions (or moles) to recognize melanoma is the current norm in clinical practice [2, 3]. Dermatologists spent significant time overseeing skin infections and seeing patients for worries regarding new or changing moles and lesions. Explicit elements are to be distinguished under the dermoscopy and the highlights are organized by utilizing approved calculations to assist with deciding the gamble of melanoma [4] by the dermatologists. Nonetheless, the large number of dermoscopic highlights and calculations are intricate, confounding, and dreary to recognize [5]. Thusly, numerous dermatologists don't use dermoscopic instruments appropriately or precisely, which might cause compromised clinical consideration. Different imaging strategies, for example, multispectral imaging and confocal microscopy, have been executed to resolve the issues experienced in the discovery of melanomas. Be that as it may, such imaging gadgets are exorbitant and cumbersome, and the dermatologist must be prepared for these imaging modalities. It is shown that dermoscopic assessment via prepared and experienced

DOI: https://doi.org/10.54216/IJNS.190113
Received: May 03, 2022 Accepted: August 08, 2022

dermatologists yields better responsiveness and particularity [6] in skin lesion findings. Subsequently, a programmed method for vigorous examination of the dermoscopic dataset can be profitable to clinicians.

The segmentation task is utilized to distinguish the areas and limits of lesions, though the grouping task is utilized to analyze their kinds of them (for example melanoma, nevus, seborrheic keratosis, and so forth). The two undertakings are trying because of three reasons: (1) the low differentiation between every lesion and its encompassing skin tissue brings about fluffy lesion limits; (2) the between-type skin lesions might share visual similitudes, and the intra-type lesions might have visual contrasts; and (3) skin lesions fluctuate essentially in the visual appearance, which might be adulterated by antiques like hair, veins, and air bubbles [7]. The advantage of segmentation to grouping is self-evident since the segmentation results give the locale of interests (ROIs), in which the discriminative elements can be extricated. Be that as it may, the arrangement interaction depends on and delivers just the data of image-level class names. Deep learning has significantly worked on the cutting edge in object arrangement and item identification. The DCNN has additionally been broadly utilized on the biomedical dataset, for example, for skin lesion examination [8-10]. Various elements distinguished at the different convolutional layers permit the organization to deal with enormous varieties in the dataset. It empowers the element location to be dealt with consequently, subsequently enhancing the challenges of component discovery

Xie et al. [11] proposed a new skin cancer classification technique, named MB-DCNN technique. It involves a coarse segmentation network (coarse-SN), a mask-guided classifier network (mask-CN), and an enhanced segmentation network (enhanced-SN). Next, Khan et al. [12] developed a novel optimal color feature (OCF) of and DCNN model to segment and classify skin lesions. This hybrid approach aimed to eradicate the artifacts and enhance the contrast level of the lesions. Afterward, colro segmentation approach is developed and the outcome of the OCF model can be improvised using a saliency model. The DCNN-9 technique can be designed for deriving deeper features and integrated into the OCFs using a fusion model. Khouloud et al. [13] proposed another DL model to detect and classify melanoma. It comprises three stages namely pre-processing, segmentation, and classification with two DL models namely W-net and Inception Resnet. In [14], another DL model with segmentation and classification processes is presented. At the time of segmenting lesions, the contrast level can be enhanced via fusing two filtering techniques and carrying out a color conversion to color lesion area color judgment. Then, optimal channels are chosen and the lesion mapping can be determined that can be again transformed to binary values via the thresholding process. To classify lesions, two pre-trained CNN models are applied.

This article introduces a Neutrosophic C-Means Clustering with Optimal Machine Learning Enabled Skin Lesion Segmentation and Classification (NCCOML-SKSC) model. The proposed NCCOML-SKSC model derives a NCC-based segmentation approach to segment the dermoscopic images. Besides, the AlexNet model is exploited to generate a feature vector. In the final stage, the optimal multilayer perceptron (MLP) model is utilized for the classification process in which the MLP parameters are chosen by the use of a whale optimization algorithm (WOA). A detailed experimental analysis of the NCCOML-SKSC model using a benchmark dataset is performed.

2. Design of NCCOML-SKSC Technique

In this study, a new NCCOML-SKSC model has been developed for the effectual segmentation and classification of skin cancer using dermoscopic images. The proposed NCCOML-SKSC technique encompasses pre-processing, NCC-based segmentation, AlexNet feature extraction, MLP classification, and WOA parameter optimization. The MLP parameters are optimally chosen by the use of WOA.

2.1 The process involved in NCC-based Segmentation

At the time of segmentation, the NCC model receives the pre-processed skin lesion images and identifies the affected regions that exist in them. The NCM is utilized in finding the indeterminacy values among various intensity groups which undergo segmentation. Every $W(x, y)$ in the image can be defined in the NS domain based on membership function (MF) as given below [15]:

DOI: https://doi.org/10.54216/IJNS.190113
Received: May 03, 2022 Accepted: August 08, 2022

$$W_{NS}(x,y) = \{T(x,y), I(x,y), F(x,y)\} \quad (1)$$

where the $T(x,y)$, $I(x,y)$ and $F(x,y)$ denotes the members belonging to the forefront, indeterminate set, and backdrop, correspondingly. Consider a dataset $X = \{x_i, i = 1,2,\dots,N\}$, the correct and indeterminacy membership subsets of pixels n_i at point i can be defined as $T_{NCM-n_{ij}}$ and l_{NCM-n_i}, correspondingly as given below:

$$T_{NcM-n_{ij}} = \frac{Q}{w_1}\left(x_i - c_j\right)^{-\frac{2}{m-1}} \quad (2)$$

$$I_{NcM-n_i} = \frac{Q}{w_2}\left(x_i - \overline{c}_{i\,\max}\right)^{-\frac{2}{m-1}} \quad (3)$$

where x_i denotes an instance in d- dimension space. For c clusters, c_j characterizes the cluster centers. In the NCM, the objective function undergoes minimization as given below.

$$Q = \left[\frac{1}{w_1}\sum_{j=1}^{c}\left(x_i - c_j\right)^{-\frac{2}{m-1}} + \frac{1}{w_2}\left(x_i - \overline{c}_{i\,\max}\right)^{-\frac{2}{m-1}} + \frac{1}{w_3}r^{\frac{2}{m-1}}\right]^{-1} \quad (4)$$

where w_1, w_2, and w_3 are weight factors, and r represents a control parameter. In addition, $\overline{c}_{i\,\max}$ is determined using indexes of the largest and second- largest $T_{ij\,Value}$. At every round, the repeated procedure in the NCM gets upgraded till the given constraints are satisfied:

$$|T^{(k+1)}_{NCM-n_j} - T^{(k)}_{NCM-n_j}| < l \quad (5)$$

where l denotes the least constant number for the termination condition.

2.2 AlexNet-based Feature Extraction

During the feature extraction process, the AlexNet model is used to generate feature vectors. AlexNet is a commonly employed model, which contains eight layers: five convolutional layers, two fully-connected hidden layers, and one fully-connected output layer [16]. Second, AlexNet used the ReLU instead of the sigmoid as its activation function. It is widely applied for image recognition, object detection, etc. In this work, the AlexNet model is utilized to create feature vectors from dermoscopic images.

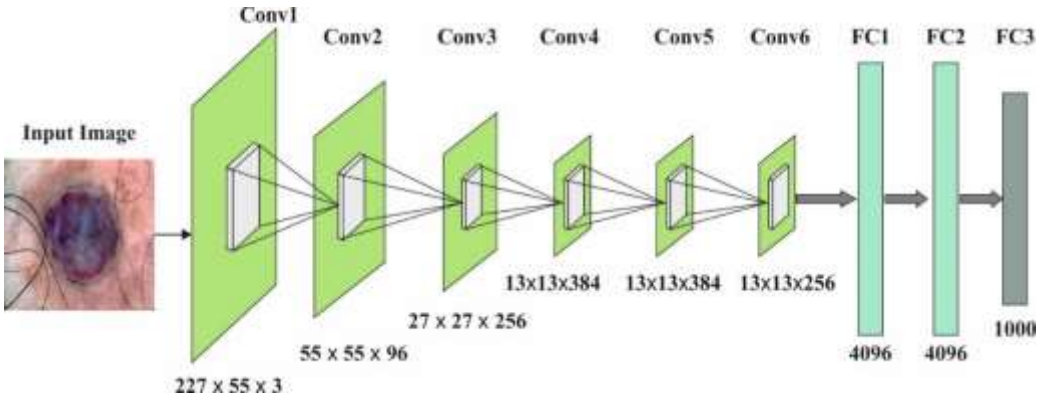

Figure 1: Structure of AlexNet model

2.3 MLP Classifier

In the classification of skin lesion images, the MLP model is used to properly assign class labels to it [17]. MLP is determined as the class of feedforward ANN by means of 3 layers. The basic structure of MLP is proved in involves n, h, and m to indicate the amount of input, hidden, and output nodes. After

DOI: https://doi.org/10.54216/IJNS.190113
Received: May 03, 2022 Accepted: August 08, 2022

that, the weight of MLP is stored in a W matrix and the bias is noted in matrix B. The MLP output evaluated is shown below. Firstly, the weighted sum of inputs is evaluated by,

$$s_j = \sum_{i=1}^{n} (W((j-1)n+i) * I_i) + B(j), j = 1,2,\cdots,h \quad (6)$$

$W((j-1)n+i)$ denotes weight from ith input nodes to jth hidden nodes, $B(j)$ indicates the bias of jth hidden nodes, and I_i denotes the ith input. Here [17], weight and bias are anticipated in a matrix form whereby it characterizes the storing in matrix format. After that, the experiment result at the hidden layer is given as follows

$$S_j = sigmoid\ (s_j) = \frac{1}{(1+\exp(-s_j))}, j = 1,2,\cdots,h \quad (7)$$

Lastly, the resulting outcomes are defined,

$$o_k = \sum_{j}^{h} (W(nh+(k-1)h+j) * S\ + B(h+k),$$

$$k = 1,2,\cdots,m \quad (8)$$

$$O_k = sigmoid(o_k) = \frac{1}{(1+\exp(-o_k))}, k = 1,2,\cdots,m \quad (9)$$

$W(nh+(k-1)h+j)$ implies the weight from the jth layer in the hidden node to the kth layer in the output node and $B(h+k)$ signifies the bias of the kth output layer. The main goal is to train MLP and accomplish the best weight-bias incorporation from the input. In the problem representation, the weight and bias incorporate a candidate with a population whereby biases and weights are measured as a candidate solution.

$$Candidate\ Solution\ = \{W(1),\cdots\cdots W(nh+mh), B(1),\ldots,B(h+m)\} \quad (10)$$

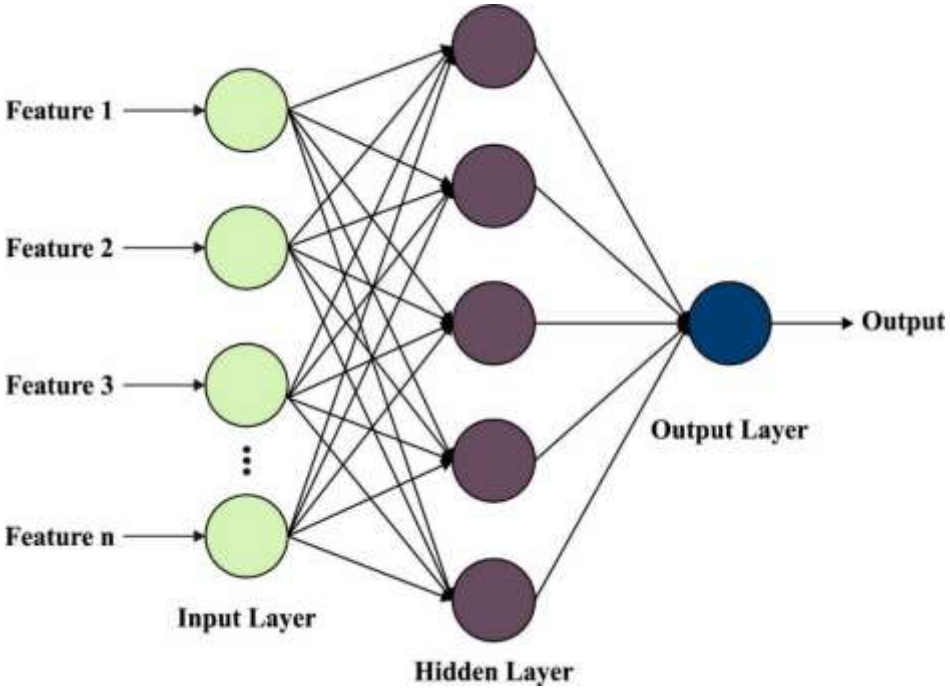

Figure 2: Structure of MLP model

DOI: https://doi.org/10.54216/IJNS.190113
Received: May 03, 2022 Accepted: August 08, 2022

The number of weights should be enhanced as $nh + mh$ and the total amount of biases must be improved as $h + m$. Henceforth, the number of attributes enhanced for the MLP training can be characterized as $(n + 1)h + (h + 1)m$. Typically, the structure of MLP is represented as $n - h - m$.

Here, input is measured as an attribute. Consequently, the sum total of input layers is equal to the sum total of features in classifier problems. No rules are utilized to choose the hidden layer, and rules are employed in our work,

$$H = 2XN + 1 \tag{11}$$

N and H show the count of the input and hidden nodes. The total weights to be augmented are $nh + mh$ and the sum total of biases augmented is $h + m$.

2.4 WOA-based Parameter Tuning

In order to optimally tune the MLP parameters, the WOA is utilized and it improves the classification performance [18]. In WOA, 2 models are advanced to denote the arithmetical value of bubble-net behavior of humpback whales called as exploitation stage in which this framework is shown below:

Encircling Prey. When the location of prey is recognized, they enclose it and surround them. Firstly, the position of the plan in a searching region hasn't been explored; therefore, the WOA considered a leading candidate solution is a targeted prey. After that, an alternative searching agent accomplishes to adapt the location to the optimum searching agent:

$$\vec{\mathrm{E}}(\mathrm{n}+1) = \overrightarrow{\mathrm{E}^*}(\mathrm{n}) - \vec{\mathrm{A}} \cdot \vec{\mathrm{D}}, \tag{12}$$

$$\vec{\mathrm{D}} = |\vec{\mathrm{C}} \cdot \overrightarrow{\mathrm{E}^*}(\mathrm{n}) - \vec{\mathrm{E}}(\mathrm{n})|, \tag{13}$$

Whereas $\overrightarrow{\mathrm{E}^*}(\mathrm{n})$ indicates the whale location on iteration n. $\vec{\mathrm{E}}(\mathrm{n}+1)$ denotes the whale's current position, $\vec{\mathrm{D}}$ signifies the distance vector between prey and whale, $||$ characterizes accurate value. The C and A denotes coefficient vector defined in the following:

$$\vec{\mathrm{A}} = 2 \cdot \vec{\mathrm{a}}\vec{\mathrm{r}} + \vec{\mathrm{a}}, \tag{14}$$

$$\vec{\mathrm{C}} = 2 \cdot \vec{\mathrm{r}}. \tag{15}$$

Spiral Updating Position. In distance between a whale suited from (E, Y) and victim position of $(\mathrm{E}^*, \mathrm{F}^*)$ is minimized. Now, a spiral function is formed between the position of the victim and the whale to reflect the helix-shaped way of the humpback whale as follows:

$$\vec{\mathrm{E}}(\mathrm{n}+1) = \mathrm{e}^{\mathrm{bk}} \cdot \cos(2\pi\mathrm{k}) \cdot \overrightarrow{\mathrm{D}^*} + \overrightarrow{\mathrm{E}^*}(\mathrm{n}), \tag{16}$$

$$\overrightarrow{\mathrm{D}^*} = |\overrightarrow{\mathrm{E}^*}(\mathrm{n}) - \vec{\mathrm{E}}(\mathrm{n})|, \tag{17}$$

Here b indicates a constant value to discover the architecture of a logarithmic spiral and k implies an arbitrary number $[-1, 1]$. This nature is indicated in WOA for adapting the whale place in optimization. Maximal possibility for choosing a reduction encircling and spiral technique wherein the module is established consequently:

$$\vec{\mathrm{E}}(\mathrm{n}+1) = \begin{cases} \overrightarrow{\mathrm{E}^*} - \vec{\mathrm{A}} \cdot \vec{\mathrm{D}}, & \text{if } \mathrm{p} < 0.5, \\ \mathrm{e}^{\mathrm{bk}} \cdot \cos(2\pi\mathrm{k}) \cdot \overrightarrow{\mathrm{D}^*} + \overrightarrow{\mathrm{X}^*}(\mathrm{n}), & \text{if } \mathrm{p} \geq 0.5, \end{cases} \tag{18}$$

Now p signifies an arbitrary number within (0, 1).

Search for Prey. The search technique is called as exploration stage. It depends upon the modification of $\overrightarrow{\mathrm{the\,A}}$ vector. It aims to calculate global searching and solve the local optimum topics. The arithmetical method is portrayed in the equation:

$$\vec{\mathrm{E}}(\mathrm{n}+1) = \overrightarrow{\mathrm{E}_{\mathrm{rand}}} - \vec{\mathrm{A}} \cdot \vec{\mathrm{D}}, \tag{19}$$

DOI: https://doi.org/10.54216/IJNS.190113
Received: May 03, 2022 Accepted: August 08, 2022

$$\vec{D} = \left|\vec{C} \cdot \overrightarrow{E_{rand}} - \vec{E}\right|, \quad (20)$$

In which $\overrightarrow{E_{rand}}$ denotes the arbitrary location vector designated from the current population.

3. Results and Discussion

The performance validation of the NCCOML-SKSC model is performed using a skin lesion dataset. Fig. 3 shows sample dermoscopic images.

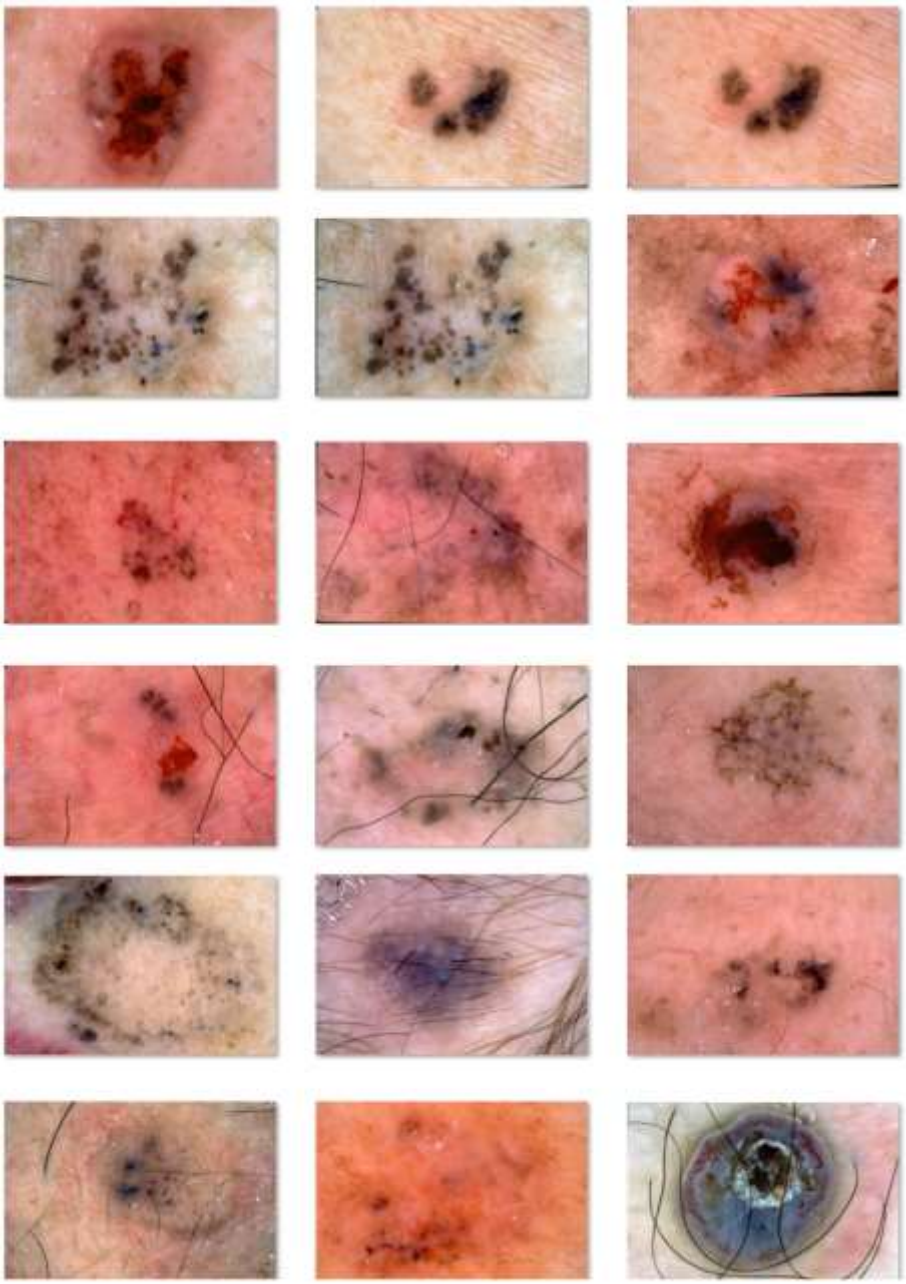

Figure 3: Sample images

Table 1 and Fig. 4 inspect the outcome of the NCCOML-SKSC model in terms of the number of clusters. The results indicated that the NCCOML-SKSC model has depicted effectual performance with minimal clusters under all images compared to other models. For instance, with image 1, the NCCOML-SKSC model has attained 2 clusters whereas the OHBCE-NCM GC, HBC-NCMGC, and HBCE-NCM models have achieved 3, 3, and 2 clusters. Similarly, with image 2, the NCCOML-SKSC

DOI: https://doi.org/10.54216/IJNS.190113
Received: May 03, 2022 Accepted: August 08, 2022

model has reached 2 clusters whereas the OHBCE-NCM GC, HBC-NCMGC, and HBCE-NCM models have attained 3, 3, and 2 clusters. Likewise, with image 3, the NCCOML-SKSC model has reached 2 clusters whereas the OHBCE-NCM GC, HBC-NCMGC, and HBCE-NCM models have achieved 3, 3, and 2 clusters. Moreover, with image 4, the NCCOML-SKSC model has accomplished 2 clusters whereas the OHBCE-NCM GC, HBC-NCMGC, and HBCE-NCM models have achieved 4, 4, and 2 clusters. Furthermore, with image 5, the NCCOML-SKSC model has gotten 2 clusters whereas the OHBCE-NCM GC, HBC-NCMGC, and HBCE-NCM models have completed 4, 4, and 3 clusters.

Table 1: No. of Cluster analysis of the NCCOML-SKSC model

No. of Images	NCCOML-SKSC	Optimal HBCE-NCM GC	HBC-NCMGC	HBCE-NCM
Image-1	2	3	3	2
Image-2	2	3	3	2
Image-3	2	3	3	2
Image-4	2	4	4	2
Image-5	2	4	4	3
Image-6	2	5	5	3
Image-7	3	6	5	4
Image-8	3	5	5	5
Image-9	4	5	5	5
Image-10	2	4	4	3

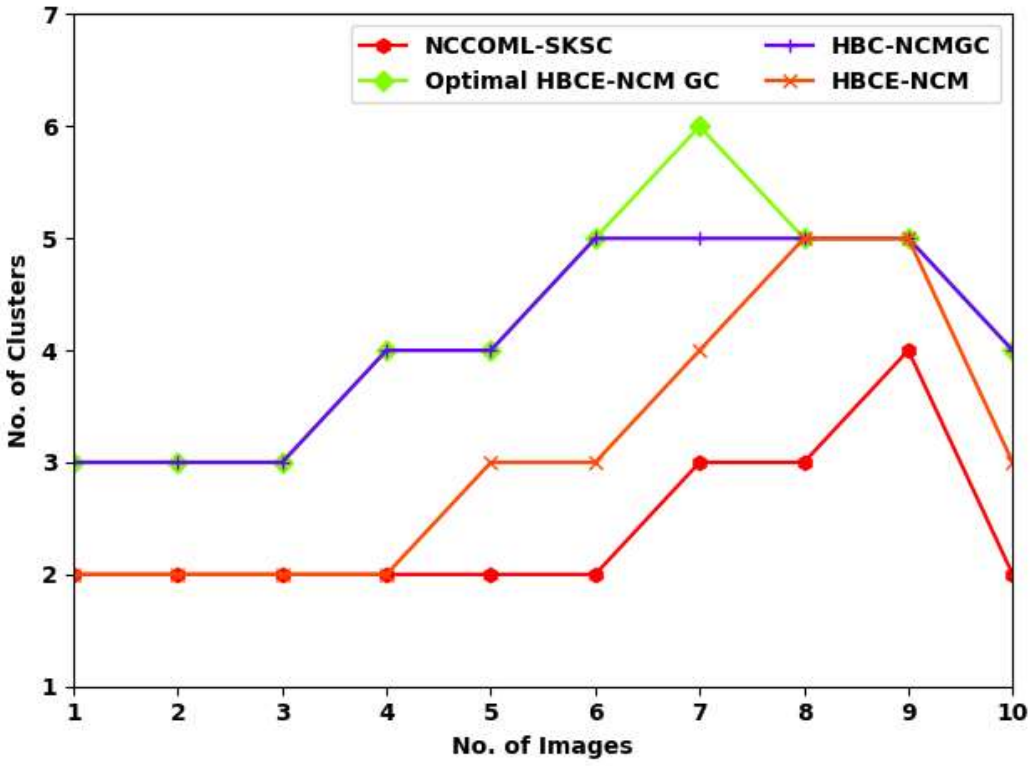

Figure 4: Comparative Cluster analysis of the NCCOML-SKSC model

Next, Table 2 and Fig. 5 portray the Jaccard Index (JI) inspection of the NCCOML-SKSC model with other models. The table values revealed that the NCCOML-SKSC model has accomplished maximum values of JI under all images. For instance, with image 1, the NCCOML-SKSC model has offered JI of

DOI: https://doi.org/10.54216/IJNS.190113
Received: May 03, 2022 Accepted: August 08, 2022

91.72% whereas the OHBCE-NCM GC, HBC-NCMGC, and HBCE-NCM models have attained JI of 83.94%, 79.08%, and 78.59% respectively. Along with that, with image 2, the NCCOML-SKSC model has offered JI of 92.94% whereas the OHBCE-NCM GC, HBC-NCMGC, and HBCE-NCM models have attained JI of 86.62%, 39.94%, and 39.21% respectively. At the same time, with image 3, the NCCOML-SKSC model has offered JI of 94.39% whereas the OHBCE-NCM GC, HBC-NCMGC, and HBCE-NCM models have attained JI of 85.64%, 81.51%, and 80.29% respectively. Meanwhile, with image 4, the NCCOML-SKSC model has offered JI of 95.61% whereas the OHBCE-NCM GC, HBC-NCMGC, and HBCE-NCM models have attained JI of 84.91%, 66.20%, and 65.71% respectively.

Table 2: JI examination of the NCCOML-SKSC model

No. of Images	NCCOML-SKSC	Optimal HBCE-NCM GC	HBC-NCMGC	HBCE-NCM
Image-1	91.72	83.94	79.08	78.59
Image-2	92.94	86.62	39.94	39.21
Image-3	94.39	85.64	81.51	80.29
Image-4	95.61	84.91	66.20	65.71
Image-5	97.07	88.80	73.73	81.51
Image-6	99.26	96.10	51.85	41.16
Image-7	98.28	93.42	44.08	52.34
Image-8	97.31	93.66	41.40	40.19
Image-9	93.91	87.10	68.63	66.68
Image-10	91.96	81.75	51.12	48.45

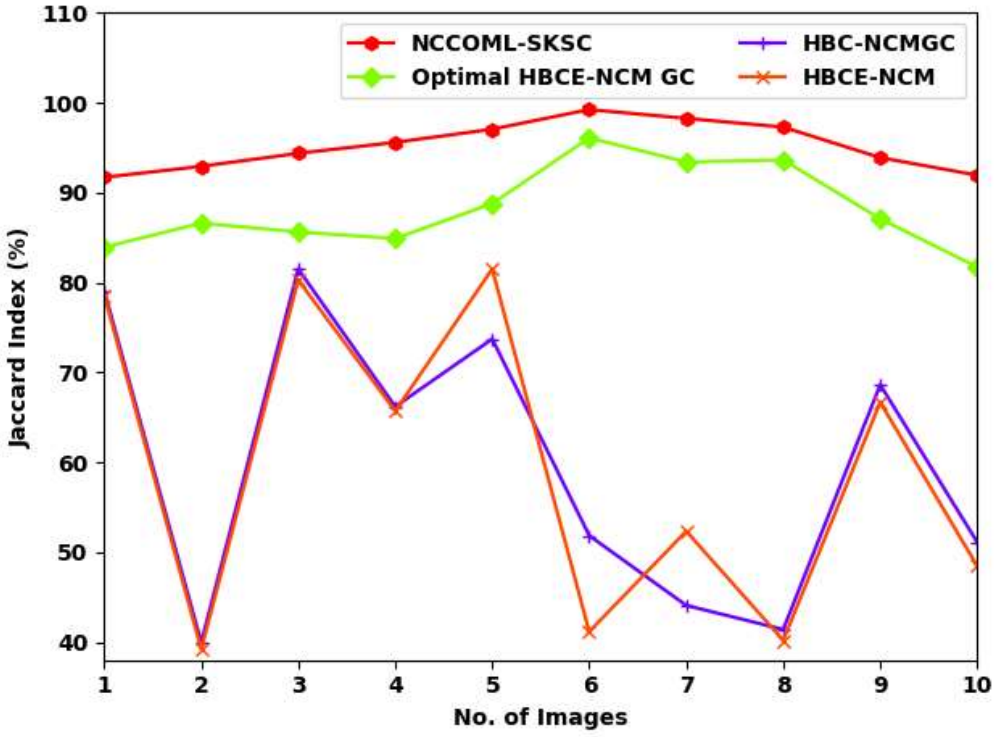

Figure 5: Comparative JI assessment of the NCCOML-SKSC model

In order to report the enhanced outcomes of the NCCOML-SKSC model, a comparative inspection is made with recent methods [19] in Table 3 and Fig. 6. The experimental values indicated that the GC model has gained lower performance with $sens_y$, $spec_y$, $accu_y$, JI, and dice of 78.69%, 85.10%,

DOI: https://doi.org/10.54216/IJNS.190113
Received: May 03, 2022 Accepted: August 08, 2022

80.54%, 57.86%, and 85.64% respectively. At the same time, the HBCE-NCMGC model has obtained slightly enhanced outcomes with $sens_y$, $spec_y$, $accu_y$, JI, and dice of 94.38%, 86.47%, 92.68%, 59.75%, and 90.57% respectively. Moreover, the HBCE-NCM model has accomplished moderately $sens_y$, $spec_y$, $accu_y$, JI, and dice of 95.32%, 88.37%, 94.21%, 59.41%, and 89.26% respectively. However, the NCCOML-SKSC model has accomplished an effectual outcome with maximum $sens_y$, $spec_y$, $accu_y$, JI, and dice of 97.68%, 97.38%, 98.24%, 95.24%, and 95.38% respectively. After looking into the tables and figures, it is depicted that the NCCOML-SKSC model has showcased effectual results over the other methods.

Table 3: Comparative study of the NCCOML-SKSC model

Methods	Sensitivity	Specificity	Accuracy	Jaccard Index	Dice
GC	78.69	85.10	80.54	57.86	85.64
HBCE-NCM	95.32	88.37	94.21	59.41	89.26
HBC-NCMGC	94.38	86.47	92.68	59.75	90.57
Optimal HBCE-NCMGC	95.11	87.54	96.31	88.20	92.69
NCCOML-SKSC	97.68	97.38	98.24	95.24	95.38

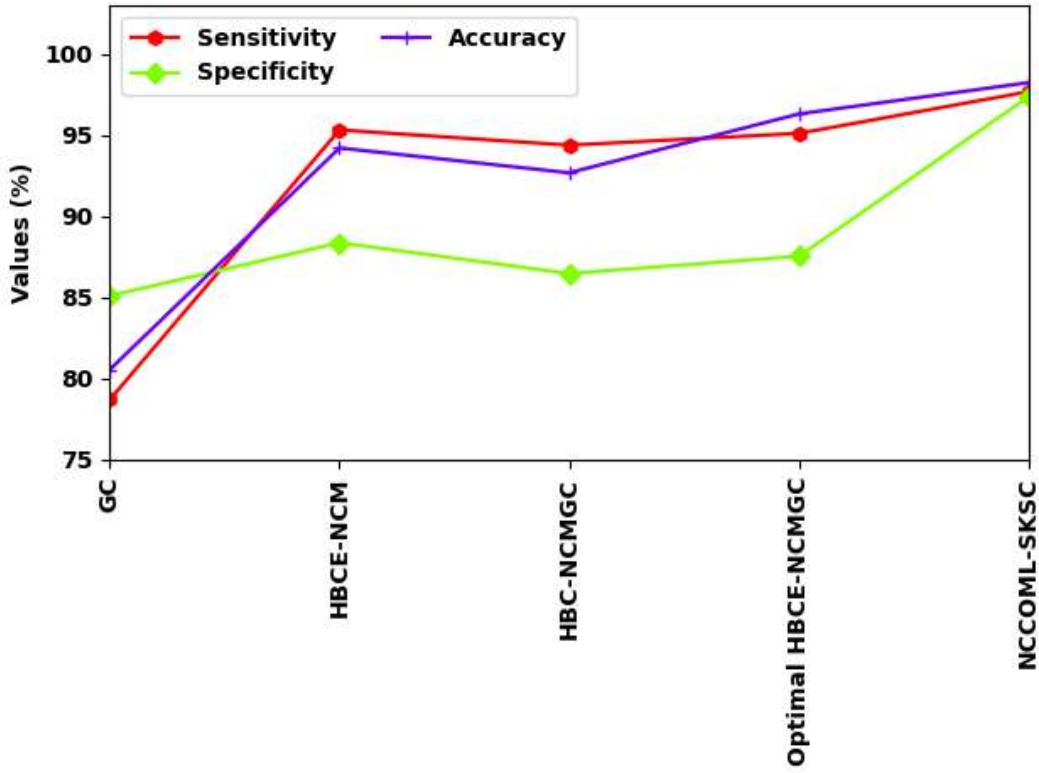

Figure 6: Comparative classification outcomes of the NCCOML-SKSC model

4. Conclusion

In this study, a new NCCOML-SKSC model has been developed for the effectual segmentation and classification of skin cancer using dermoscopic images. The proposed NCCOML-SKSC technique encompasses pre-processing, NCC-based segmentation, AlexNet feature extraction, MLP classification,

DOI: https://doi.org/10.54216/IJNS.190113
Received: May 03, 2022 Accepted: August 08, 2022

and WOA parameter optimization. The MLP parameters are optimally chosen by the use of WOA. A detailed experimental analysis of the NCCOML-SKSC model using a benchmark dataset is performed and the results are inspected under dissimilar aspects. The experimental outcome highlighted the better performance of the NCCOML-SKSC model over the other methods. In the future, the NCCOML-SKSC technique can be extended to DL-based classification models.

References

[1] Yang, X., Zeng, Z., Yeo, S.Y., Tan, C., Tey, H.L. and Su, Y., 2017. A novel multi-task deep learning model for skin lesion segmentation and classification. arXiv preprint arXiv:1703.01025.

[2] Baig, R., Bibi, M., Hamid, A., Kausar, S. and Khalid, S., 2020. Deep learning approaches towards skin lesion segmentation and classification from dermoscopic images-a review. Current Medical Imaging, 16(5), pp.513-533.

[3] Bissoto, A., Perez, F., Ribeiro, V., Fornaciali, M., Avila, S. and Valle, E., 2018. Deep-learning ensembles for skin-lesion segmentation, analysis, classification: RECOD titans at ISIC challenge 2018. arXiv preprint arXiv:1808.08480.

[4] Chen, J., Chen, J., Zhou, Z., Li, B., Yuille, A. and Lu, Y., 2021. MT-TransUNet: Mediating Multi-Task Tokens in Transformers for Skin Lesion Segmentation and Classification. arXiv preprint arXiv:2112.01767.

[5] Liu, L., Tsui, Y.Y. and Mandal, M., 2021. Skin lesion segmentation using deep learning with the auxiliary task. Journal of Imaging, 7(4), p.67.

[6] Khan, A.H., Iskandar, D.A., Al-Asad, J.F. and El-Nakla SAMIRAnd Alhuwaidi, S.A., 2021. Statistical Feature Learning through Enhanced Delaunay Clustering and Ensemble Classifiers for Skin Lesion Segmentation and Classification. Journal of Theoretical and Applied Information Technology, 99(5).

[7] Mohammed I. Alghamdi, Neutrosophic set with Adaptive Neuro-Fuzzy Inference System for Liver Tumor Segmentation and Classification Model, International Journal of Neutrosophic Science, Vol. 18 , No. 2 , (2022) : 174-185

[8] Sireesha Rodda , Vaibhav Kovela , Sanjay Dokula, Instance Segmentation and Labeling of Teeth from Dental X-Ray using Region Based Convolutional Neural Network, Journal of Neutrosophic and Fuzzy Systems, Vol. 2 , No. 2 , (2022) : 20-30

[9] Jabbar Abed Eleiwy, Characterizing wavelet coefficients with decomposition for medical images, Journal of Intelligent Systems and Internet of Things, Vol. 2 , No. 1 , (2021) : 26-32

[10] Reshma, G., Al-Atroshi, C., Nassa, V.K., Geetha, B., Sunitha, G., Galety, M.G. and Neelakandan, S., 2022. Deep Learning-Based Skin Lesion Diagnosis Model Using Dermoscopic Images. Intell. Autom. Soft Comput, 31, pp.621-634.

[11] Sundus Naji AL-Aziz , Reem Atassi , Abd Al-Aziz Hosni El-Bagoury, Hybridization of Neutrosophic Logic with Quasi-Oppositional Chimp Optimization based Data Classification Model, International Journal of Neutrosophic Science, Vol. 18 , No. 3 , (2022) : 125-134

[12] Khan, M.A., Sharif, M.I., Raza, M., Anjum, A., Saba, T. and Shad, S.A., 2019. Skin lesion segmentation and classification: A unified framework of deep neural network features fusion and selection. Expert Systems, p.e12497.

[13] Khouloud, S., Ahlem, M., Fadel, T. and Amel, S., 2022. W-net and inception residual network for skin lesion segmentation and classification. Applied Intelligence, 52(4), pp.3976-3994.

[14] M. F.O. Noboa , O. E.P. Copa , Eloísa A.N. G., Comparative analysis of multicriteria methods based on single-valued neutrosophic numbers for the evaluation of medical technologies, International Journal of Neutrosophic Science, Vol. 18 , No. 4 , (2022) : 72-82

[15] Dhar, S. and Kundu, M.K., 2021. Accurate multi-class image segmentation using weak continuity constraints and neutrosophic set. Applied Soft Computing, 112, p.107759.

[16] Kalaiarasi, P. and Esther Rani, P., 2021. A Comparative Analysis of AlexNet and GoogLeNet with a Simple DCNN for Face Recognition. In Advances in Smart System Technologies (pp. 655-668). Springer, Singapore.

[17] Andino Maseleno, Design of Optimal Machine Learning based Cybersecurity Intrusion Detection Systems, Journal of Cybersecurity and Information Management, Vol. 0 , No. 1 , (2019) : 32-43

DOI: https://doi.org/10.54216/IJNS.190113
Received: May 03, 2022 Accepted: August 08, 2022

[18] Chakraborty, S., Saha, A.K., Sharma, S., Mirjalili, S. and Chakraborty, R., 2021. A novel enhanced whale optimization algorithm for global optimization. Computers & Industrial Engineering, 153, p.107086.

[19] Hawas, A.R., Guo, Y., Du, C., Polat, K. and Ashour, A.S., 2020. OCE-NGC: A neutrosophic graph cut algorithm using an optimized clustering estimation algorithm for dermoscopic skin lesion segmentation. Applied Soft Computing, 86, p.105931.

DOI: https://doi.org/10.54216/IJNS.190113
Received: May 03, 2022 Accepted: August 08, 2022